United model for low-cycle, high-cycle and giga-cycle fatigue life prediction

N.S. Selyutina [1,2] ✉ iD, Yu.V. Petrov [1,2] iD

[1] St. Petersburg State University, St. Petersburg, Russia

[2] Institute for Problems in Mechanical Engineering of the Russian Academy of Science, St. Petersburg, Russia

✉ nina.selutina@gmail.com

ABSTRACT
The methods for determining the cyclic strengths of metals under low-cycle and high-cycle fatigue are different, since the mechanisms of failure and the extent of the presence or absence of plastic deformation differ for each type of fatigue. The aim of this study is to develop united models for both low-cycle and high-cycle fatigue life prediction. We propose that the relevant relaxation and damage processes are considered and it on different types of metals is tested. In this paper, the cyclic deformation of materials is considered using the proposed model with regard to two processes: stress relaxation and damage accumulation kinetics. Proposed approach allows us to study the united fatigue curves of materials regardless of the chosen type of fatigue (low-cycle fatigue, high-cycle fatigue, giga-cycle fatigue). Fatigue life curves under staircase strain loading and symmetrical sinusoidal strain/stress loading are predicted in this study. A simple numerical scheme for the model is successfully applied to various materials under various types of loading, since the relaxation–kinetic model is phenomenological in nature.

KEYWORDS
fatigue strength • metals • inelastic adaptability • fatigue life curve • short-term strength • long-term strength

Introduction

The appearance and propagation of fatigue cracks in materials often cause disasters, and to prevent fatigue failure, it is necessary to evaluate fatigue life of materials. The Wöhler curve is a graphical representation illustrating the relationship between cyclic stress amplitude and the number of cycles to failure (N) for a material that fails as a result of mechanical cycling. This curve is critical to understanding the fatigue behaviours of materials, especially metals. It helps engineers and materials scientists to develop components and structures that can withstand cyclic loads over long periods of time. The fatigue life curve usually includes three characteristic zones: low-cycle, high-cycle and giga-cycle fatigue (Fig. 1). Past research shows that for low-cycle fatigue, the dominant mechanism is associated with plastic deformation and the initiation of various defects, including crack-like defects. The stresses are fairly high level in nature, and the macroscopic fracture of the material occurs after a relatively small number of cycles. In this case, fracture is often accompanied by both the accumulation of plastic deformation and the growth of cracks. For high-cycle fatigue, the initiation and cumulative growth of damage, including crack-like defects, become more significant. This process occurs at
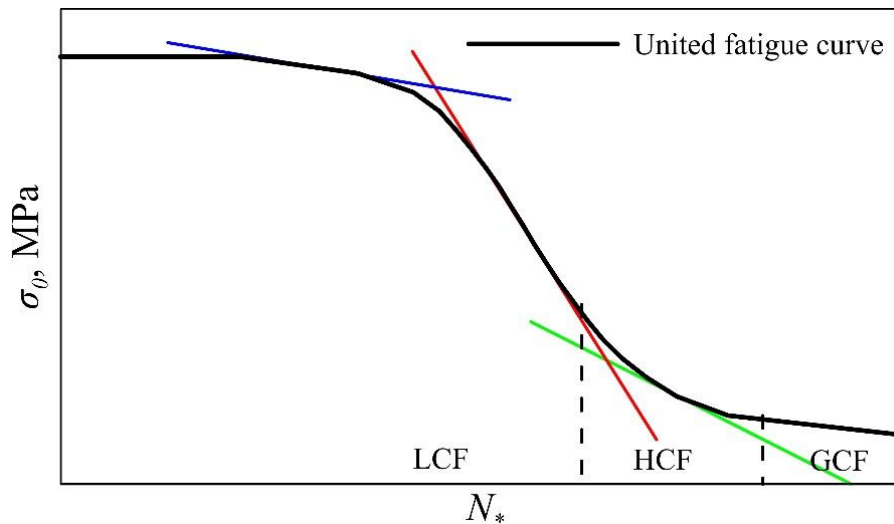
Fig. 1. The dependence of cyclic strength on the number of cycles before failure and its conditional sections within the following zones: LCF is low-cycle fatigue; HCF is high-cycle fatigue; GCF is giga-cycle fatigue

medium-level stress amplitudes, with a moderate number of cycles occurring until the macro-fracture of the material. Both plastic deformation and defect growth contribute to failure. In ultra-high-cycle fatigue, visible damage and cracks are usually caused by internal defects in the material and surface peculiarities. The stress level is of low amplitude, and the rupture of the medium mainly occurs due to the sudden growth of small cracks after a large number of cycles. Studies reviewing past work on low-cycle [1,2] and high-cycle [3–5] fatigue highlighted the diversity of existing approaches and the lack of a unified approach for calculating fatigue life.

For each section of the curves of low-cycle, high-cycle and giga-cycle fatigue, various models have been formulated, including empirical models [6–10], residual stress relaxation models [11–14] and kinetic equations [15–18]. The latter are usually associated with predicting the crack propagation process related to the intermediate stage of fatigue failure between crack initiation, which is invisible to the observer, and final fracture due to the rapid acceleration of crack growth. As noted in [11,12,19], in addition to the processes of fatigue failure, there are relaxation processes associated with the accumulation of plastic deformation in the material. In this case, models are usually formulated separately, and these models take into account the initiation and growth of cracks and other models associated with the relaxation processes of plastic deformation. This study proposes combining the stress relaxation process and the evolution of damage accumulation to predict the complete Wöhler fatigue curve.

A relaxation model of cyclic deformation has been formulated previously [20,21], explicitly taking into account the ongoing relaxation processes in the material by introducing a characteristic relaxation time and a stress relaxation function. In previous studies, the proposed model was verified to predict the effects of low-cycle deformation. It was shown that this model is particularly capable of simultaneously predicting the effects of the stabilisation of plastic deformation and the full deformation response of the material across the entire cyclic loading regime. In conventional approaches [1–5], the effect of the deformation amplitude on the deformation response of the material is taken into account

by the linear movement of the hysteresis curve, in contrast to the proposed model, where the deformation response is obtained automatically.

In this paper, based on the relaxation model of cyclic deformation, a fatigue life model of relaxation and damage (FLMRD) is formulated to predict the effects of cyclic deformation for a wide range of cycle numbers, ranging from low-cycle to giga-cycle fatigue. To verify the Wöhler curve, the model is supplemented with the Kachanov–Rabotnov damage equation [15,17], which improves the performance of the original model beyond the stabilising cycle. Theoretical fatigue dependencies for steels are plotted using experimental data derived from the literature as an example.

Fatigue life model of relaxation and damage

Experiments on low-cycle and high-cycle fatigue show the different dependences of the ultimate stress (cyclic strength σ_0) on the cycle number before failure: the so-called fatigue life curve. Existing models used in engineering practice for determining the fatigue life curve are often empirical in nature [9,10]. In this paper, we propose a fatigue life model combining relaxation and damage (FLMRD) that can automatically and simultaneously calculate the short-term and long-term strengths of the material.

To predict the cumulative plastic deformation in a material, we propose using a relaxation model modified for a cyclic process [20,21] with an additional fracture condition. The purpose of the combined FLMRD model in the proposed work is to explicitly take into account the relaxation processes of the force field during cyclic deformation, as well as consider the process of damage accumulation. The combined model assumes that there are three possible cases of cyclic deformation of the material. In the first case, the material undergoes elastic–plastic deformation and there is no stabilisation of plastic deformation, since there is a consistent accumulation of plastic deformation cycle after cycle until the deformation of the material occurs. In the second case—low-cycle fatigue up to $\sim 5 \cdot 10^4$ cycles— the material undergoes elastic–plastic deformation until plastic deformation is stabilised occurs and the material collapses, accumulating critical damage in the material cycle after cycle. In the third case, giga-cycle fatigue, first, the material deforms almost elastically, and then deforms after achieving a stabilisation effect, as in the second case. In the proposed combined model, elastoplastic deformation is predicted using a relaxation model for cyclic deformation [20,21], and the damage accumulation process is predicted using the Kachanov–Rabotnov-type equation [15,17]. The transition point between the two models is taken to be a non-zero initial condition for the damage parameter ω_0, calculated using the relaxation model of cyclic deformation when the material reaches the stabilising cycle of plastic deformation N_{stab}. Thus, in the first case, the calculation is carried out using only the relaxation model for cyclic deformation [20,21], whereas in the second and third cases, it is carried out using both models. Let us consider in more detail the calculation scheme before ($N < N_{stab}$) and after ($N > N_{stab}$) the beginning of the stabilising cycle of plastic deformation.

Relaxation model of plasticity

In the relaxation model of plastic deformation [22,23], the specimen is deformed to $\varepsilon(t) = \varphi(t) H(t)$, where $H(t)$ is the Heaviside function, and $\varphi(t)$ is the strain-time function. The dimensionless function of relaxation $0 < \gamma(t) \leqslant 1$ is introduced:

$$\gamma(t) = \begin{cases} 1, & \frac{1}{\tau}\int_{t-\tau}^{t}\left(\frac{\Sigma(s)}{\sigma_y}\right)^{\alpha} ds \leq 1, \\ \left(\frac{1}{\tau}\int_{t-\tau}^{t}\left(\frac{\Sigma(s)}{\sigma_y}\right)^{\alpha} ds\right)^{-1/\alpha}, & \frac{1}{\tau}\int_{t-\tau}^{t}\left(\frac{\Sigma(s)}{\sigma_y}\right)^{\alpha} ds > 1, \end{cases} \tag{1}$$

where τ is the incubation time, α is the sensitivity factor of the material to the load amplitude, $\Sigma(t) = E\varepsilon(t)$ is the stress-time function, σ_y is the static yield stress, and t is time.

The equality $\gamma(t)$ in Eq. (1) is related to inelastic strain accumulation prior to macroscopic yield at t_*, determined from the condition of equality to one integral condition in Eq. (1). A decrease in the relaxation function in the range $0 < \gamma(t) < 1$ corresponds to the transition of the material to the plastic deformation stage. During plastic deformation $t \geqslant t_*$, the condition is met for $\gamma(t)$:

$$\frac{1}{\tau}\int_{t-\tau}^{t}\left(\frac{\gamma(t)\Sigma(s)}{\sigma_y}\right)^{\alpha} ds = 1. \tag{2}$$

Equality (2) is retained due to fixing state at the initial yield $t = t_*$. The calculation scheme for t_* is given in [11], and subsequent relaxation of elastic stresses are accumulated in the material ($0 < \gamma(t) < 1$). We determine the true stresses in the deformed specimen at $t \geqslant t_*$ in the following form:

$$\sigma(t) = \begin{cases} E\varepsilon(t), & t < t_*, \\ E\varepsilon(t)\gamma(t)^{1-\beta}, & t \geq t_*. \end{cases} \tag{3}$$

where E is Young's modulus, and β is the dimensionless scalar parameter ($0 \leqslant \beta < 1$), which describes the degree of material hardening. For $\beta = 0$, no hardening occurs. Young's modulus is determined from static experiments. We propose that Young's modulus is an invariant to loading history. A whole series of monotonic and monotonous deformation dependencies is predicted [22,23].

Relaxation model of cyclic deformation ($N < N_{stab}$)

To predict the cumulative plastic deformation in a material, we propose using a relaxation model of plastic deformation [22,23], modified for a cyclic process [20,21]. The main essence of the proposed relaxation model of cyclic deformation (CRM) is to explicitly take into account the relaxation process in the material.

The equation of the true stresses of the material using the model in [20,21] for the j-th cycle up to $N < N_{stab}$ is presented in the following form:

$$\sigma_j\left(\varepsilon_j(t)\right)\Big|_{N<N_{stab};W<W_*} = \begin{cases} \sigma\left(\varepsilon_j(t)\right), & t < t_j^{unl}, \\ E\left(\varepsilon_j(t) - \varepsilon_j^{unl}\right)H\left(\varepsilon_j(t) - \varepsilon_j^{unl}\right), & t \geq t_j^{unl}. \end{cases} \tag{4}$$

where $\sigma_j(\varepsilon_j(t))$ is the stress time dependence, $\varepsilon_j(t)$ is the current strain time dependence, t_j^{unl} is the unloading time, ε_j^{unl} is the strain at t_j^{unl}, N_{stab} is the number of stabilising cycles in the material, and t_* is the fracture time. The stress–strain relationship in true coordinates $\sigma(\varepsilon_j(t))$ at each j cycle is determined using the relaxation plasticity model [20,21].

$$\sigma\left(\varepsilon_j(t)\right) = \begin{cases} E\varepsilon_j(t), & t < t_y^j, \\ E\left[\gamma_j(t)\right]^{1-\beta}\varepsilon_j(t), & t \geq t_y^j, \end{cases} \tag{5}$$

with the stress relaxation function on the j-th cycle:

$$\gamma_j(t) = \begin{cases} 1, & \frac{1}{\tau}\int_{t-\tau}^{t}\left(\frac{\Sigma(s)}{\sigma_y^j}\right)^{\alpha}ds \leq 1, \\ \left(\frac{1}{\tau}\int_{t-\tau}^{t}\left(\frac{\Sigma(s)}{\sigma_y^j}\right)^{\alpha}ds\right)^{-1/\alpha}, & \frac{1}{\tau}\int_{t-\tau}^{t}\left(\frac{\Sigma(s)}{\sigma_y^j}\right)^{\alpha}ds > 1. \end{cases} \tag{6}$$

As noted in [22,23], the cyclic yield strength is less than the static yield strength; therefore, in the calculation scheme, we consider σ_y^j to be the static yield strength for samples subjected to cyclic loads.

The yield condition at the j-th cycle is determined by the following yield criterion [24]:

$$\frac{1}{\tau}\int_{t_y^j-\tau}^{t_y^j}\left(\frac{\Sigma(s)}{\sigma_y^j}\right)^{\alpha}ds = 1. \tag{7}$$

At the $(j+1)$-th cycle, the static yield strength is determined by the following condition:

$$\sigma_y^{j+1} + \sigma_y^j = 2\left|\sigma_j\left(\varepsilon_j\left(t_j^{unl}\right)\right)\right|, \tag{8}$$

where $\sigma_y^0 = \sigma_y$. We assume that the time and cycle number are related by the ratio $t = N/v$, where v is the loading frequency [16].

Using the relaxation model of cyclic deformation (CRM) (4)–(7), with explicit consideration of the ongoing relaxation processes, makes it possible to predict the cumulative plastic strain and volumetric strain energy density in the current cycle. When the plastic deformation is stabilised, the model allows us to evaluate the cyclic strength of the material as the maximum stress of the material on the hysteresis loop, and the corresponding cycle number is N_{stab}.

To calculate the fracture moment when a material reaches cyclic strength σ_0, we propose to use the condition of equality in the following energy criterion (fracture criterion):

$$W(t) \leq W_*, \tag{9}$$

where W is the volumetric strain energy density, and W is the strain energy density under quasi-static loads. The parameter W is defined as the area of the subgraph of the resulting deformation response of the material, calculated using the relaxation model of cyclic deformation (Eqs. (4)–(7)):

$$W_j = \int \sigma_j(\varepsilon_j)d\varepsilon_j. \tag{10}$$

At each cycling step, the change in the cumulative damage parameter is calculated through the cumulative volumetric deformation energy density W_j at the j-th cycle of the material:

$$\omega_j = \frac{\sum_{k=1}^{j} W_k}{W_*}. \tag{11}$$

Kinetic damage equation ($N > N_{stab}$)

In order to determine the number of the cycle before the fracture of the material (N_*) with a steady-stabilising cycle of plastic deformation ($N > N_{stab}$), it is necessary to use the generalised damage equation [17] of the Kachanov–Rabotnov type [15] with the damage parameter $0 \leq \omega \leq 1$, defined as follows:

$$\frac{d\omega}{dN} = \frac{A(\sigma_0)^a}{v}\frac{\omega^b}{(1-\omega)^a}, \tag{12}$$

σ_0 is the given time stress function, *a*, *b* and *A* are constants. At the beginning of the stabilisation mode N_{stab}, damage ω_0 accumulates in the material. The damage parameter ω_0 is determined by $\omega_0 = W_{stab}/W_*$, being the ratio of the volumetric strain energy density W_{stab} cumulating in a stable cycle N_{stab} to the volumetric strain energy density under quasi-static loads W_*. The volumetric strain energy density per cycle is defined as the area of the subgraph of the deformation diagram calculated using the relaxation model for cyclic deformation. We assume that σ_0 = const is a constant value, determined, using the relaxation model of plasticity in the stabilising cycle, to be the maximum stress of the material on the hysteresis loop.

To solve Eq. (12), a non-zero initial condition ω_0 is assumed, as was the case in the article of [25]:

$$\omega|_{N=N_{stab}} = \omega_0, \tag{13}$$

where ω = 1 at the moment of fracture $N = N_*$ and the damage parameter is equal to 1. Separating the variables, we integrate Eq. (6) over time from N_{stab} to N_* as follows:

$$N_* = N_{stab}(\sigma_0) + \frac{1}{A\sigma_0}\left(1 - \frac{1}{\omega_0^2}\right)\frac{\Gamma(a+1)\Gamma(1-b)}{\Gamma(a-b+2)}, \tag{14}$$

where $\Gamma(x)$ is the gamma function, defined at $x > 0$ as:

$$\Gamma(x) = \int_0^\infty s^{x-1}e^{-s}ds. \tag{15}$$

Then, using Eqs. (4)–(15), it is possible to costruct the dependence of the critical stress before failure σ_0 on the cycle number N_* (or the fatigue *S-N* dependence).

General purpose of the FLMRD model

The main benefit of using the FLMRD model is its simultaneous consideration of two competing processes of plastic deformation and fracture. Its explicit representation of the relaxation function (6) makes it possible to predict the process of plastic deformation. A non-zero initial condition for the damage parameter allows us to estimate the history of the accumulated level of damage (12) in the material when there is no influence of plastic deformation.

Figure 2(a) shows a united fatigue curve for a hypothetical material in logarithmic coordinates under the staircase loading method. By drawing two tangent lines to the inclined portion of the fatigue curve, as shown in Fig. 1, it is possible to identify the stages of low-cycle fatigue (up to $2 \cdot 10^4$ cycles), high-cycle fatigue (from $2 \cdot 10^4$ to $3 \cdot 10^7$ cycles) and ultra-high-cycle fatigue (after $3 \cdot 10^7$ cycles). These three stages are plotted using the FLMRD model with a fixed set of parameters. Figure 2(b) plots the dependence of the cycle number at which new plastic deformations do not accumulate, N_{stab}, on the number of cycles before failure, *N*, for a hypothetical material, for which the united fatigue curve is shown in Fig. 2(a).

Each cyclic strength σ_0 corresponds to a cycle number N_{stab}. As shown in Fig. 2(a), with a decrease in the cyclic strength, the cycle number N_{stab} decreases, but the number of cycles before failure N_* increases. At $N \sim 4 \cdot 10^7$ cycles, the material deforms elastically, since N_{stab} = 1. At $N < 4 \cdot 10^7$, the material undergoes elastic–plastic deformation. The application of the evolutionary damage equation (7) allows us to "shift" the results on cyclic strength and N_{stab} obtained from the relaxation plasticity model (1)–(6) to the right and obtain the final united fatigue curve. In other words, using a combination of methods

(a)

(b)
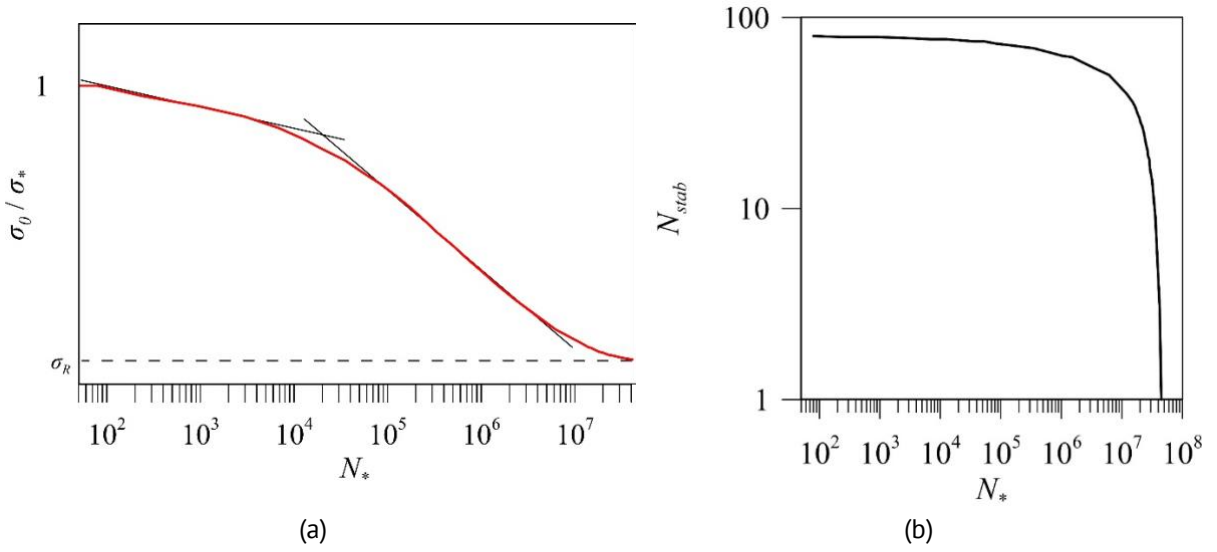
Fig. 2. (a) Dependence of the cyclic strength, normalised to the static strength of the hypothetical material, on the number of cycles for the hypothetical material. (b) The dependence of the cycle number at which new plastic deformations do not accumulate, N_{stab}, on the number of cycles before failure N for a hypothetical material

and obtain the final united fatigue curve. In other words, using a combination of methods to explicitly take into account relaxation processes and the process of damage accumulation, it becomes possible to construct united fatigue curve, including a continuous inclined section of a united fatigue curve that is important for engineering practice.

Prediction of cyclic strength of metals before ~10^6 cycle

In this section, the proposed model is used to predict the cyclic strength under low-cycle and high-cycle fatigue. Let us assess the performance of the proposed combined model with experimental data on soft loading for the two-phase steel DP500 [26], where σ_y^0=350 MPa and σ_* =570 MPa, and X65 steel [27], where σ_y^0=420 MPa and σ_* =620 MPa. The cyclic deformation in [26] was carried out based on the sinusoidal tensile load at a frequency of 10 Hz under the following conditions: the minimum stress was 0 and the average stress was half the maximum stress. Previously, based on the same experimental data, it was predicted that plastic deformation would be stabilised [20]. The evaluated parameters of the model were obtained as $\alpha = 1$, $\tau = 0.67$ ms, $\beta = 0.067$, $a = 1$ and $b = 1$ for DP500 steel and $\alpha = 1$, $\tau = 1$ ms, $\beta = 0.05$, $a = 1$ and $b = 1$ for X65 steel (Table 1). For the selected set of parameters of the combined model, we can calculate the dependence of the fracture time on the stabilisation time by integrating Eq. (12):

$$N_* = t_{stab}(N_*) + \frac{1}{A\sigma_0}(\omega_0 - 1 - ln\omega_0). \tag{16}$$

Figure 3 and 4 show the theoretical fatigue relationship for DP600 dual-phase steel and X65 steel, which is in good agreement with the experimental data. Figure 3 and 4 show that the combined model can predict the complete dependence of the ultimate stress before failure based on the number of cycles, both for low-cycle and high-cycle
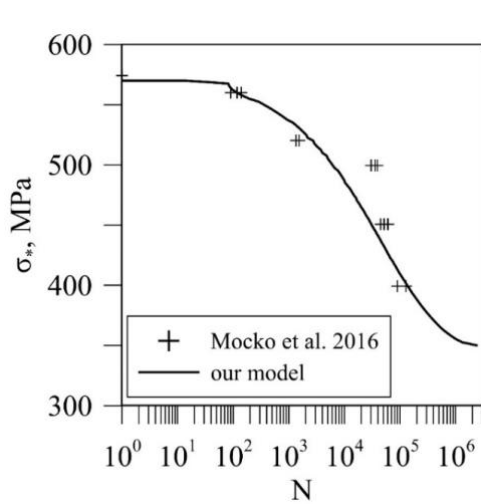
Fig. 3. A prediction of the united fatigue curve of DP500 steel based on the relaxation model of irreversible deformation during cyclic deformation, and experimental data [26]
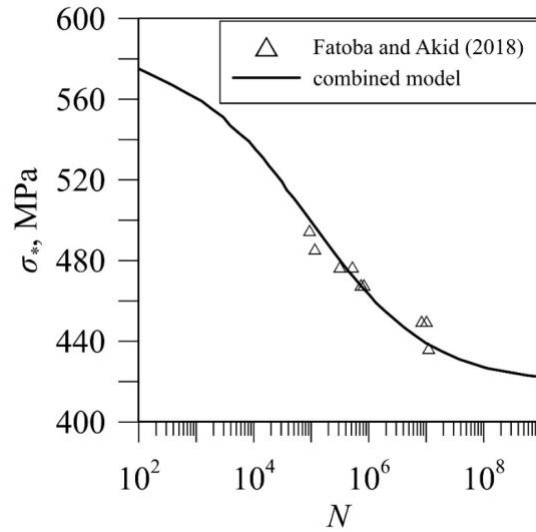
Fig. 4. A prediction of the united fatigue curve of X65 steel based on the relaxation model of irreversible deformation during cyclic deformation and experimental data [27]

Table 1. The parameters of DP500 and X65 steel for the calculation of the fatigue curve

	α	τ	β	W	A	a	b	σ_y^0	σ_*
	–	Ms	–	J	1/(MPa·s)	–	–	MPa	MPa
DP500 steel	1	0.67	0.067	2.495	0.01	1	1	350	570
X65 steel	1	1	0.05	2.494	0.01	1	1	420	620

deformation. It is commonly believed that the boundary between low-cycle and high-cycle fatigue occurs at ~ $5 \cdot 10^4$ cycles. Within the framework of the combined model, there is no need for a clear division of cases into low-cycle and high-cycle fatigue, since a united fatigue dependence is predicted for the material.

Let us consider the possibility of predicting the number of cycles before failure depending on the deformation amplitude using 34CrNiMo6 [28–31]. The loading mode used in [28–31] is strain control at the symmetrical cycle. The best agreement with experimental data is achieved using the following parameters: E = 209 GPa, α = 1, β = 0.23, σ_y^0 = 600 MPa, σ_f = 1180 MPa, A = 14, W_0 = 440, a = 1.2 and b = 1.68 (Table 2). The proposed model successfully predicts the number of cycles until fatigue failure at a given strain amplitude in the low-cycle and high-cycle fatigue ranges (Fig. 5). Note that the predicted united fatigue curve is based on experimental data covering a range of cycles to failure.

Table 2. The parameters of 34CrNiMo6 steel for the calculation of the fatigue curve

|	α	τ	β	W	A	a	b	σ_y^0	σ_*
	–	Ms	–	J	1/(MPa·s)	–	–	MPa	MPa
34CrNiMo6	1	0.23	0.067	440	14	1.2	1.68	600	1180
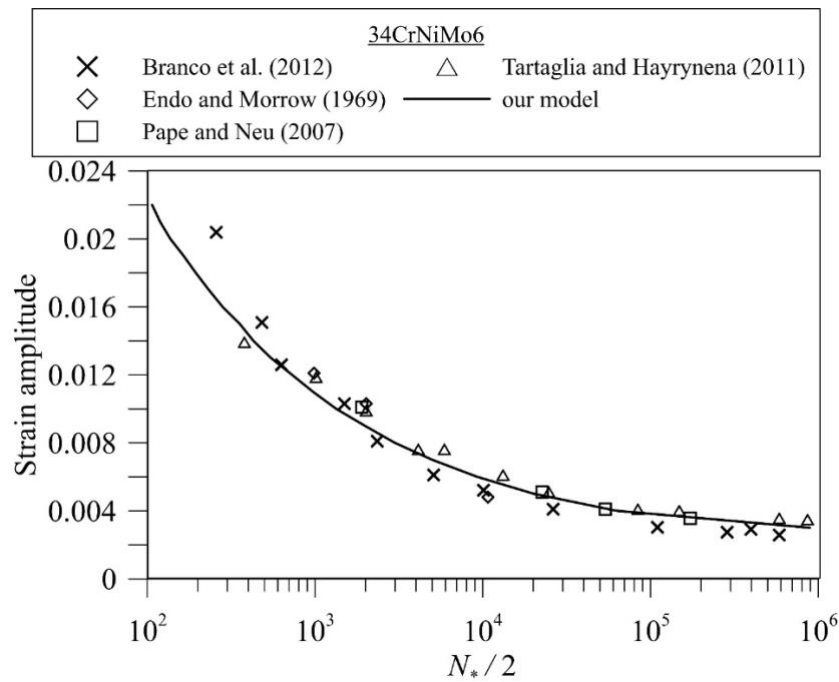
Fig. 5. A prediction of the fatigue curve (Wöhler diagram) of 34CrNiMo6 based on the relaxation model of irreversible deformation during cyclic deformation, and experimental data [28–31]

Prediction of united fatigue life curve based on FLMRD model

In this section, we consider the action of the FLMRD model with fatigue life curves, introduced in the "Fatigue life model of relaxation and damage" section. Examples of the low-cycle, high-cycle and giga-cycle fatigue life prediction for A2017-T4 aluminium alloy, 7075-T651 aluminium alloy, Ti-6Al-4V titanium alloy are shown in Figs. 6–9. Experimental data for A2017-T4 aluminium alloy [32], 7075 aluminium alloy [33,34], Ti-6Al-4V [35,36] and 300M steel [34] have been received in symmetrical compression/tension cyclic mode ($R = -1$). Parameters α, τ and β were obtained based on the assessment of deformation responses under both quasi-static and cyclic loading, presented in the corresponding experimental works [32–36]. The remaining parameters of the KDE model were selected based on the united fatigue life curves of the materials [32–36]. The best agreement with experimental data is achieved using the parameters, presented in Table 3. Significant differences in the parameters of the KDE model W_* and A are observed. The theoretical curves in Figs. 6–9 match both sections of the experimental curve well for short-term and long-term strengths within the framework of the FLMRD model, without focusing on the type of cyclic strength with a greater or lesser amount of plastic deformation. The theoretical unite fatigue curve is plotted up to 10^8 for aluminium alloys and up to 10^9 cycles for Ti-6Al-4V titanium alloy. Calculation of the deformation energy from the deformation response made it possible to set the initial condition for the kinetic equation of the model and simultaneously calculate both the short-term and long-term strength of metals. The presented kinetic-relaxation model can be applied to other materials and cyclic loading modes.

Table 3. The parameters of materials for the fatigue life prediction based on FLMRD model

Loading type	α	τ	E	β	W	A	a	b	σ_y^0	σ_*
	–	ms	GPa	–	J	(MPa·s)$^{-1}$	–	–	MPa	MPa
A2017	1	0.5	72	0.13	23	0.1	1.2	2.2	107	440
Ti-6Al-4V	1	0.3	127	0.15	190	150	1.4	2	170	1100
AA7075	1	0.5	72	0.15	18	0.3	1.25	2	131	632
M300 steel	1	0.7	210	0.15	190	40	1.4	2	680	1600
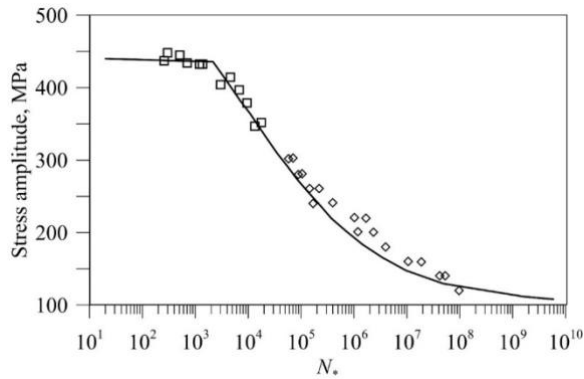
Fig. 6. A prediction of the fatigue life curve of A2017-T4 aluminium alloy based on FLMRD model and experimental data [32]
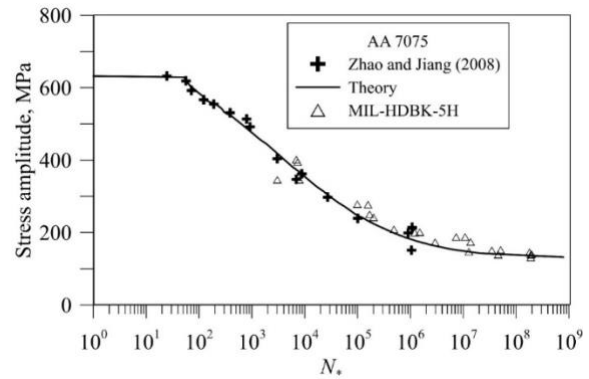
Fig. 7. A prediction of the fatigue life curve of 7075-T651 aluminium alloy based on FLMRD model and experimental data [33,34]
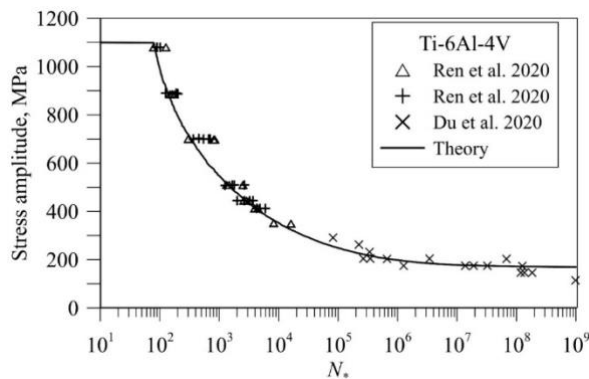
Fig. 8. A prediction of the fatigue curve (Wöhler diagram) of Ti-6Al-4V titanium alloy based on the relaxation model of irreversible deformation during cyclic deformation, and experimental data [35,36]
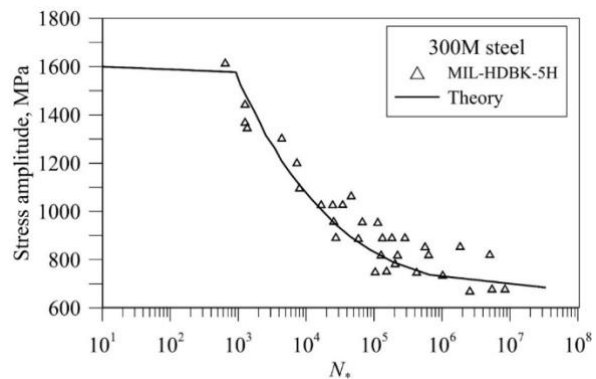
Fig. 9. A prediction of the fatigue curve (Wöhler diagram) of 300M steel based on the relaxation model of irreversible deformation during cyclic deformation, and experimental data [34]

Conclusions

An analysis of two fatigue dependencies was carried out: the short-term and long-term strengths of steels and the amplitude of deformations, both depending on the number of cycles before failure.

A predictive FLMRD model was established to estimate the united fatigue curve. The united theoretical fatigue curves of steel 45, DP 500 steel, X65 steel, 34CrNiMo6 steel, A2017-T4 aluminium alloy, 7075 aluminium alloy, Ti-6Al-4V and 300M steel show that the developed FLMRD model can serve as a convenient tool for modelling short-term and long-term strengths.

The FLMRD model can be used for the calculation of the number of cycles before fracture, cyclic strength, irreversible energy deformation (current, at the moment of the

completion of plastic deformation and at the moment of final brittle failure), accumulated irreversible deformation and the amount of cumulative damage.

The necessity of simultaneous consideration of the damage accumulation process under cyclic loads and the relaxation processes of plastic deformation is highlighted, and this can be carried out by considering the characteristic relaxation times of a given material.

CRediT authorship contribution statement

Nina S. Selyutina 🆔Sc℞°: writing – review & editing, writing – original draft, conceptualization, analysis of the result, investigation; **Yuri V. Petrov** 🆔Sc℞°: writing – original draft, the main idea, state of the problem, conceptualization, combining model, analysis of the result, supervision.

Conflict of interest

The authors declare that they have no conflict of interest.

References

1. Lakshmi S, Prabha DC. A Review on Low Cycle Fatigue Failure. *International Journal of Science Technology and Engineering.* 2017;3(11): 77–80.
2. Xu Y, Li X, Zhang Y, Yang J. Ultra-Low Cycle Fatigue Life Prediction Model – A Review. *Metals.* 2023;13(6): 1142.
3. Jeddi D, Palin-Luc T. A review about the effects of structural and operational factors on the gigacycle fatigue of steels. *Fatigue and Fracture of Engineering Materials and Structures.* 2018;41(5): 969–990.
4. Sakai T. Historical review and future prospect for researcher on very high cycle fatigue of metallic materials. *Fatigue and Fracture of Engineering Materials and Structures.* 2023;46(4) 1217–1255.
5. Hectors K, Waele WD. Cumulative Damage and Life Prediction Models for High-Cycle Fatigue of Metals: A Review. *Metals.* 2021;11(2): 204.
6. Basquin OH. The exponential law of endurance tests. *Proceedings-American Society for Testing and Materials.* 1910;10: 625–630.
7. Arutyunyan AR. Influence of aging on fatigue strength of carbon fiber reinforced plastics. *Materials Physics and Mechanics.* 2024;52(1): 118-125.
8. Arutyunyan AR, Arutyunyan RA. Damage and fracture of viscous-plastic compressible materials. *Materials Physics and Mechanics.* 2020;44(2): 250-255.
9. Murakami Y, Takagi T, Wada K, Matsunaga H. Essential structure of S-N curve: Prediction of fatigue life and fatigue limit of defective materials and nature of scatter. *International Journal of Fatigue.* 2021;146: 106138.
10. Klemenc J, Fajdiga M. Joint estimation of E-N curves and their scatter using evolutionary algorithms. *International Journal of Fatigue.* 2013;56: 42-53.
11. Benedetti M, Fontanari V, Scardi P, Ricardo CLA, Bandini M. Reverse bending fatigue of shot peened 7075–T651 aluminium alloy: The role of residual stress relaxation. *International Journal of Fatigue.* 2009;31(8–9): 1225–1236.
12. Zhuang WZ, Halford GR. Investigation of residual stress relaxation under cyclic load. *International Journal of Fatigue.* 2001;23: S31–37.
13. Jhansale HR, Topper TH. Engineering analysis of the inelastic stress response of a structural metal under variable cyclic strains. *Cyclic stress–strain behavior–analysis, experimentation, and failure prediction.* American Society for Testing and Materials ASTM; 1973. p.246–270.
14. Kodama S. The behavior of residual stress during fatigue stress cycles. In: *Proceedings of the international conference on mechanical behavior of metals II.* Kyoto (Japan); 1972. p.111–118.
15. Rabotnov YuN. *Problems of Strength of Materials and Structures.* Moscow: Izd. Akad. Nauk SSSR: 1959. (In Russian)

16. Arutyunyan AR. Formulation of the fatigue fracture criterion of composite materials. *Vestnik of Saint Petersburg University. Mathematics. Mechanics. Astronomy.* 2020;7(3): 511–517 [in Russian].

17. Stepanova LV, Igonin SA. Rabotnov damage parameter and description of delayed fracture: Results, current status, application to fracture mechanics, and prospects. *Journal of Applied Mechanics and Technical Physics.* 2015;56: 282–292.

18. Tanaka K, Akiniwa Y. Fatigue crack propagation behaviour derived from S–N data in very high cycle regime. *Fatigue and Fracture of Engineering Materials and Structures.* 2002;25(8–9): 775–784.

19. Avilés R, Albizuri J, Rodríguez A. López de Lacalle LN. Influence of low-plasticity ball burnishing on the high-cycle fatigue strength of medium carbon AISI 1045 steel. *International Journal of Fatigue.* 2013;55: 230–244.

20. Selyutina NS, Petrov YV. Effect of plastic strain stabilisation under low-cycle deformation. *Physical Mesomechanics.* 2020;23: 384–389.

21. Selyutina NS, Smirnov IV, Petrov YuV. Stabilisation effect of strain hysteresis loop for steel 45. *International Journal of Fatigue.* 2021;145: 106133.

22. Selyutina N, Petrov YV. Instabilities of dynamic strain diagrams predicted by the relaxation model of plasticity. *Journal of Dynamic Behavior of Materials.* 2022;8: 304–315.

23. Petrov YV, Borodin EN. Relaxation Mechanism of Plastic Deformation and Its Justification Using the Example of the Sharp Yield Point Phenomenon in Whiskers. *Physics of the Solid State.* 2015;57(2): 353–359.

24. Selyutina NS, Petrov YuV. Prediction of the dynamic yield strength of metals using two structural-temporal parameters. *Physics of the Solid State.* 2018;60(2): 244–249.

25. Kashtanov AV, Petrov YuV. Energy Approach to Determination of the Instantaneous Damage Level. *Technical Physics.* 2006;51(5): 604–608.

26. Moćko W, Brodecki A, Kruszka L. Mechanical response of dual phase steel at quasi-static and dynamic tensile loadings after initial fatigue loading. *Mechanics of Materials.* 2016;92: 18–27.

27. Fatoba O, Akid R. Uniaxial cyclic elasto-plastic deformation and fatigue failure of API-5L X65 steel under various loading conditions. *Theoretical and Applied Fracture Mechanics.* 2018;94: 147–159.

28. Branco R, Costa JD, Antunes FV. Low-cycle fatigue behavior of 34CrNiMo6 high strength steel. *Theoretical and Applied Fracture Mechanics.* 2012;58(1): 28–34.

29. Endo T, Morrow J. Cyclic stress–strain and fatigue behavior of representative aircraft metals. *Journal of Materials.* 1969;4: 159–175.

30. Pape JA, Neu RW. A comparative study of the fretting fatigue behavior of 4340 steel and PH 13-8 Mo stainless steel. *International Journal of Fatigue.* 2007;29(12): 2219–2229.

31. Tartaglia J, Hayrynena KL. Comparison of fatigue properties of austempered vs quenched and tempered 4340 steel. *Journal of Materials Engineering and Performance.* 2011;21: 1008–1024.

32. Furuya Y, Nishikawa H, Hirukawa H, Nagashima N, Takeuchi E. NIMS fatigue data sheet on low- and high-cycle fatigue properties of A2017-T4 (Al-4.0Cu-0.6Mg) aluminium alloy. *Science and Technology of Advanced Materials: Methods.* 2023;3(1): 2234272.

33. Zhao T, Jiang Y. Fatigue of 7075-T651 aluminum alloy. *International Journal of Fatigue.* 2008;30(5): 834–849.

34. *Military Handbook: Metallic materials and elements for aerospace vehicle structures.* Department of Defense USA; 1998.

35. Du L, Qian G, Zheng L, Hong Y. Influence of processing parameters of selective laser melting on high-cycle and very-high-cycle fatigue behaviour of Ti-6Al-4V. *Fatigue and Fracture of Engineering Materials and Structures.* 2020;44(1): 240–256.

36. Ren YM, Lin X, Guo PF, Yang HO, Tan H, Chen J, Li J, Zhang YY, Huang WD. Low cycle fatigue properties of Ti-6Al-4V alloy fabricated by high-power laser directed energy deposition: Experimental and prediction. *International Journal of Fatigue.* 2019;127: 58–73.